Journal of Tumor

Online Submissions: http: //www.ghrnet.org/index.php/jt
DOI: 10.17554/j.issn.1819-6187.2022.10.132

Journal of Tumor 2022 July; 10(1): 590-601
ISSN 1819-6187

ORIGINAL ARTICLE

Key Players and Potential Therapies in the Development of Breast Cancer Metastasis to the Spine

Zumana Khair MbiomedSc[1], Effie Mouhtouris BSc[1], Julia L. Gregory PhD[1], Gerald M.Y. Quan MBBS PhD FRACS FAOrthA[1,2]

1 Spinal Biology Research Laboratory, Department of Surgery, The University of Melbourne, Austin Health, PO Box 5555, Heidelberg, Melbourne 3084, Victoria, Australia;
2 Spinal Surgery Unit, Department of Orthopaedics, Austin Health.

Conflict-of-interest statement: The author(s) declare(s) that there is no conflict of interest regarding the publication of this paper.

Correspondence to: Gerald Quan, Department of Surgery, Level 8, Lance Townsend Building, Austin Health, PO Box 5555, Heidelberg, Vic. 3084, Australia.
Email: gerald.Quan@austin.org.au
Tel: +61-39496-3903
Fax: +61-39496-5817

Received: May 1, 2022
Revised: June 29, 2022
Accepted: July 2, 2022
Published online: July 22, 2022

ABSTRACT

BACKGROUND: Breast cancer metastasis to the spine causes severe morbidity due to pathological fractures, spinal cord compression, pain, loss of mobility and paralysis. An improved understanding of the biology behind metastatic breast cancer growth and invasion to the bony vertebral column is essential in order to control local tumour growth and progression of metastasis.

AIM: To identify and characterise the presence of six key markers involved in spinal metastasis progression, RANKL, OPG, MMP-9, PTHrP, VEGF and IL-6. To determine the effectiveness of inhibitory agents, bisphosphonate Zoledronic Acid and RTK inhibitor Sorafenib on cancer cell growth and survival, as well as the expression of tumour markers *in vitro*.

MATERIALS AND METHODS AND RESULTS: The presence of RANKL, OPG, MMP-9, PTHrP, VEGF and IL-6 was confirmed in the cytoplasm of secondary breast cancer cell lines MDA-MB-231, MDA-MB-453 and MCF-7 *in vitro*. This was further supported by histological analysis of tumour-containing spinal sections from an established mouse model of spinal cancer. Zoledronic Acid and Sorafenib reduced proliferation rates in all cell lines and Sorafenib caused significant apoptosis of MDA-MB-231 and MDA-MB-453 cells.

CONCLUSION: This study highlights a potential role for the markers VEGF, RANKL and IL-6 in promoting breast cancer growth, bone degradation and angiogenesis during spinal metastases. Both Zoledronic Acid and Sorafenib displayed anti-tumour effects on cancer proliferation and to a lesser extent apoptosis. These findings highlight the importance of tumour and bone-derived factors and their therapeutic application in breast cancer spinal metastasis.

Key words: Breast cancer; Metastases; Spine; Bone; Animal model

Khair Z, Mouhtouris E, Gregory JL, Quan GMY. Key Players and Potential Therapies in the Development of Breast Cancer Metastasis to the Spine. *Journal of Tumor* 2022; **10(1)**: 590-601 Available from: URL: http://www.ghrnet.org/index.php/jt/article/view/3290

INTRODUCTION

Breast cancer (BC) is the commonest invasive cancer in females worldwide and approximately 75% of advanced breast cancer patients develop bone metastasis, where the spine is the most frequent site[1]. This causes significant morbidity and mortality due to skeletal related events (SREs) including bone destruction, pathological fractures, pain, spinal cord compression, urinary or faecal incontinence, neurological decline, loss of mobility and paralysis[2]. Current, conventional multimodality therapies consist of surgery, radiation, chemotherapy and hormonal therapy[3]. However, these therapies are usually purely palliative and often fail to improve patient morbidity and survival due to treatment resistance, drug side effects and toxicity and local recurrence[3,4]. There is currently limited knowledge about

the bone-tumour microenvironment in metastatic breast cancer and as such a better understanding of the biology behind the growth and invasion of breast cancer cells to the spine and its correlation with disease progression is required. Novel interventions and targeted therapies are needed to control local growth of spinal cancer and delay disease progression by inhibiting metastasis pathways.

The bone is a dynamic tissue that requires a balance between bone-forming osteoblasts and bone-resorbing osteoclasts. In this process, osteoblast-produced RANKL binds to its receptor RANK on pre-osteoclasts, causing their differentiation into multinuclear, activated osteoclasts, which adhere to the bone and begin matrix degradation[5]. Osteoclast activity is inhibited by the decoy receptor osteoprotegerin (OPG), which binds to RANKL and inhibits RANKL/RANK interactions, thus maintaining a normal rate of bone growth and differentiation. However, during BC metastasis imbalanced bone remodelling via excess stimulation of osteoclast production results in the incomplete formation of resorbed bone. Thus, BC metastatic lesions are predominantly osteolytic[6]. Tumour cells, osteoblasts, osteoclasts and stromal cells present in the bone microenvironment secrete various bone-resorbing, matrix degrading and growth-stimulating factors including parathyroid hormone-related protein (PTHrP), transforming growth factor-beta (TGF-β), RANKL, interleukins (ILs), matrix-metalloproteinases (MMPs), vascular endothelial growth factor (VEGF), chemokines, cytokines, hormones and other physical factors[7]. These stimulate increased RANKL production by osteoblasts and suppress the expression of OPG and other bone-forming factors, resulting in increased RANKL/RANK interactions, excessive survival of osteoclasts and bone resorption[8].

Current literature on spinal metastasis of BC reveals various mechanisms of BC invasion, growth, angiogenesis matrix degradation and inflammation within the bone that contribute to the high incidence of bone metastasis. VEGF, which is a potent direct-acting mediator of angiogenesis for tumour survival and establishment in hypoxic tumour bone environment, has been shown to be a supporting factor for osteolytic bone degradation[9,10]. In addition, proteolytic destruction of the extracellular matrix is critical for tumour establishment in the bones of the spine, namely MMP-9 is a prominent factor at the tumour-stromal interface[11]. PTHrP is another key osteolytic factor involved in spinal metastasis and has shown to increase transactivation and expression of other factors that contributes to local osteolysis[8,12]. The inflammatory marker, IL-6 contributes to the heterogeneity of bone metastasis by regulating several pro-tumorigenic mechanisms of bone remodelling, inflammation, cell survival and proliferation[13,14].

A clinically relevant and reproducible mouse model has been established by the Spinal Biology Research Laboratory, University of Melbourne, that allows pre-clinical investigation of the pathophysiological processes and a temporo-spatial pattern of spinal cancer and subsequent neurological deficits[3,15]. Athymic nude mice were orthotopically inoculated with metastatic MDA-MB-231 human breast cancer cells into the lower thoracic spine, and in a clinical pattern similar to that in humans, all animals developed an expanding spinal tumour causing neurological dysfunction and evolving paralysis due to progressive spinal cord compression[3]. Paralysis was observed between 3 to 5 week's post-inoculation, progressing from normal gait (Score 0), to gait asymmetry (Score 1), unilateral hind limb paralysis (Score 2) and finally bilateral hind limb paralysis (Score 3).

This *in vivo* animal model also provides a suitable platform to test standard targeted therapies including the anti-resorptive, Zoledronic Acid (ZA) and anti-angiogenic, Sorafenib. ZA prevents bone breakdown by binding to mineralised bone surfaces and inducing apoptosis of overactive osteoclasts and preventing tumour adhesion to the bone matrix[16]. It has also demonstrates direct and indirect anti-cancer effects based on pre-clinical and early clinical studies[16]. Sorafenib is an oral multi-kinase inhibitor that blocks receptor tyrosine kinase (RTK) signalling, most commonly activated during malignant tumour proliferation, growth, invasion and angiogenesis[17]. Sorafenib has shown promising results for BC metastasis in pre-clinical and clinical trials and has been approved for treatment of other types of cancer[17].

In this study we examined the presence of six specific tumour and bone-derived markers RANKL, OPG, MMP-9, PTHrP, IL-6 and VEGF in both breast cancer cell lines and spinal cord tumour samples to determine whether there is a correlation between expression and the severity of disease. Additionally, we investigated the effectiveness of ZA and Sorafenib on cancer cell growth and survival, as well as on the expression of tumour markers *in vitro*.

MATERIALS AND METHODS

Tissue Culture

The human breast cancer cell line MDA-MB-231 was cultured in RPMI (Sigma, Australia), supplemented with 10% Fetal Bovine Serum (FBS) (VWR, Australia), 1% antibiotics (penicillin and streptomycin) and 1% Glutamax (Life Technologies Inc Australia), and incubated at 37°C in 5% CO_2. MDA-MB-453 and MCF-7 cells were cultured in DMEM (Sigma, Australia) and made with the above supplementations except MCF-7 cells which were grown in 20% FBS. Both were incubated at 37°C in 10% CO_2. All cells were cultured in 95 cm^2 medium sized flasks and passaged twice weekly. Cells were washed with 1XPBS and trypsinized in 0.25% Trypsin-EDTA (Gibco, Australia).

Mice and tumor inoculation

Animal procedures were performed in accordance with The University of Melbourne guidelines and approved by the Austin Health Ethics Committee. Mice were culled at different stages of paralysis (score 0 to 3) and thoracolumbar spinal tumour samples were harvested, formalin-fixed, decalcified and embedded in paraffin wax using methods previously established[3]. Microtome-cut 5 µm sections were heated in 37°C and mounted onto Superfrost plus slides (Thermo Scientific) and dried in a 37°C oven overnight. Sections were used for histological analysis and immunohistochemistry.

Immunohistochemistry

For Haematoxylin & Eosin (H&E) staining, spinal tissue sections were dewaxed and rehydrated in a series of xylene (Chem supply, Gillman, SA) and ethanol (100%, 70% and 30%). Harris Haematoxylin (1:3; Sigma Aldrich, Australia) was added for one minute, then prior to adding 1% Eosin Y (BDH, Australia) for 20 seconds Scott's tap water was added for blueing. Slides were dehydrated in ethanol (70% and 100%) and xylene. Coverslips were placed on the sections immediately using DePeX mounting medium (BDH, Australia). Slides were dried overnight in a fume-hood before imaging on a Nikon Coolscope II. For detection of markers using immunohistochemistry, scored spinal sections were dewaxed and rehydrated as per H&E staining. Antigen retrieval was performed in Glycine (50 µM, pH 3.5) and endogenous peroxidise activity was blocked with 3% H_2O_2 for 30 minutes. Washes were done in TBS (0.5 M, pH 7.5) and non-specific binding was blocked for 30 minutes with 5% normal animal serum. Slides were incubated overnight in a humidifying chamber at 37°C with primary antibodies: anti-RANKL, anti-OPG, anti-MMP-9, anti-PTHrP (Santa Cruz Biotech), anti-VEGF (Saphire

Bioscience) and anti-IL-6 (Abcam). Control sections received a biotin-conjugated IgG isotype at an equivalent primary antibody concentration. Sections were incubated for 60 minutes with corresponding biotinylated secondary antibodies, ant-goat IgB and anti-rabbit IgB (1:500; Santa Cruz Biotech, Australia). After incubation with a peroxidase conjugated avidin-biotin complex (Vector Elite, Burlingame, CA, USA) for 30 minutes, DAB chromogen labelling kit (Dako) was used for reaction. Samples were counterstained with haematoxylin and scott's tap water, then dehydrated in a graded series of ethanol concentrations and xylene.

WST-1 viability assay

For in vitro studies, viable cell numbers were determined using a Trypan Blue dye exclusion assay. Standardised numbers of MDA-MB-231 ($0.25x10^4$ per well), MDA-MB- 453 and MCF-7 cells ($0.5x10^4$ per well) were seeded into five 96-well plates. WST-1 dye was added at 1:10 dilution and absorbance readings were taken at 450 nm wavelength for five days by using an Optima plate reader. For treatment studies, drugs were added after 24 hours (day 0) to four of those five plates. Titrations were done for ZA at 0**µM**, 5**µM**, 25**µM**, 50**µM**, 100**µM**, 150**µM and 200µM** concentrations and for Sorafenib at 0**µM**, 10**µM**, 20**µM**, 50**µM** and 100**µM** concentrations, while cells in media were read as the control. Absorbance readings were taken each day that were compared to the initial (day 0) absorbance.

RT-PCR

RNeasy mini kit (QIAGEN, Australia) was used for RNA extraction. Homogenised cells were passed through a series of spin/discard flow-through transfers. RNeasy column was treated with RNA-ase free DNase I treatment to ensure complete removal of genomic DNA. RNA concentration and integrity were measured using the NanoDrop 2000c (Thermo Scientific, Australia). RT-PCR for GAPDH, RANKL, OPG, MMP-9, PTHrP, VEGF and IL-6 was performed using the Titanium One-Step RT-PCR kit (Clontech, USA). PCR products were separated by gel electrophoresis using 1% agarose gel containing SYBER SAFE (Invitrogen, Australia) and visualised via ethidium bromide staining using UV light with the Quantam ST4 300 system (Montreal Biotech).

Flow Cytometry

For intracellular protein analysis by flow cytometry, cells ($2x10^6$) were fixed with 2% paraformaldehyde/PBS, incubated, washed in 0.5% PBS/BSA and permeabilized using 0.5% saponin/paraformaldehyde (Sigma Aldrich, Australia). Cells were incubated on ice with RANKL (1:50), OPG (1:100), PTHrP (1:50; Santa Cruz), VEGF (1:50; Sapphire Bioscience), MMP-9 (1:50; Santa Cruz) and IL-6 (1:50; Abcam) primary antibodies diluted in 0.5% saponin/PBS for 30 minutes. After washing, FITC-conjugated secondary antibodies diluted in PBS/BSA were added: Rabbit anti-goat (1:100; Santa Cruz) for RANKL, OPG and MMP-9, Sheep anti-rabbit (1:50; Chemicon) for PTHrP and VEGF and Rabbit-anti-mouse (1:100; DAKO) for IL-6, and incubated in dark on ice for 30 minutes. Negative controls were used to detect non-specific binding. Cell samples were then run through BD FACS Canto II (Becton Dickinson, Australia), where appropriate cell populations were gated for chosen fluorescence channels. For treatment analysis, cells cultured in small flasks received ZA (0**µM**, 50**µM** and 100µM) for 72 hours and Sorafenib (0**µM**, 20**µM** and 50µM) for 24 hours following optimisations, then were analysed for RANKL, MMP-9, VEGF and IL-6 expression.

Cell proliferation assay

A cell trace CFSE proliferation kit (ThermoFisher Scientific Australia) was used to assess proliferation levels. For labelling, cells were resuspended in pre-warmed sterile 0.1% BSA/PBS and incubated in a waterbath and 4 µL of 1mM CFSE (stock) was added. Cold media washes were performed and labelled cells were aliquoted into 24-well plate ($2x10^5$ cells per well) and incubated overnight. Fluorescence (cell division) was measured by BD FACS Canto II at the same time for four consecutive days. For drug studies, after 24 hours of incubation (day 0), ZA was added at 50**µM**, 100**µM and 150µM concentrations** diluted in media and treated samples were assessed over three consecutive days. Non-labelled cells were used as negative control.

Apoptosis assay

The Annexin V-FITC Apoptosis Detection kit (Biovision, MA, USA) was used to detect Annexin V and PI-positive cells following drug treatment. Briefly, cells ($2x10^4$) were treated with ZA (0**µM**, 50**µM** and 100**µM) and** Sorafenib (0µM, 20µM and 50µM) for 72 hours, trypsinised and incubated with 300 µL reducing buffer. Annexin-5 (5 µL) and PI (5 µL) were added and incubated for 5 minutes in the dark. Cells were analysed by BD FACS Canto II. Fixed numbers of cells were gated for each sample and percentage apoptosis was quantified based on Annexin V and PI fluorescence.

Data analysis

Image J (National Institutes of Health) was used to measure and analyse the intensity of immunohistochemistry and TRAP stained sections. For each marker, positive stained region was selected and the bounds for colour, saturation and brightness parameters were kept consistent across scores 0 - 3. Mean intensity values were recorded from standard intensity results (analyse > measure) and percentage values were calculated from maximum intensity and pixel values. Four separate images from each score within each marker were chosen for analysis. All flow cytometry data were analysed through WEHI's Weasel software. Statistical software Minitab (version 16.0) was used for two-sample t tests required for flow cytometry, histology, treatment data analysis.

RESULTS

Histological analysis of MDA-MB-231-inoculated mouse spinal sections

Tissues samples from score 0 to 3 were stained with H&E. Representative images of spinal sections from different grades display increasing spinal invasion of established tumour as well as the structural changes at different stages of spinal cord compression (Figure 1). Tissues from normal mice (Score 0) consistently demonstrated complete, fully intact, symmetrical bony vertebral column containing the bone marrow and a uniform spinal canal surrounding the spinal cord (SC) (Figure 1A). Upon neurological decline, tumour growth within the vertebral body (VB) gradually invades towards the SC by destroying the bone and surrounding soft tissues, resulting in mild (Figure 1B), then moderate (Figure 1C) and ultimately severe (Figure 1D) compression of the SC. The distinct area between the SC and the cortex disappears, filling with infiltrating tumour cells; this marks the tumour-bone interface, which is the region between cortical bone and SC (Figure 1B inset).

Immunohistochemical analysis of RANKL, OPG and PTHrP expression in MDA-MB-231-Inoculated mouse spinal sections

Immunohistochemical analysis demonstrated a significant correlation

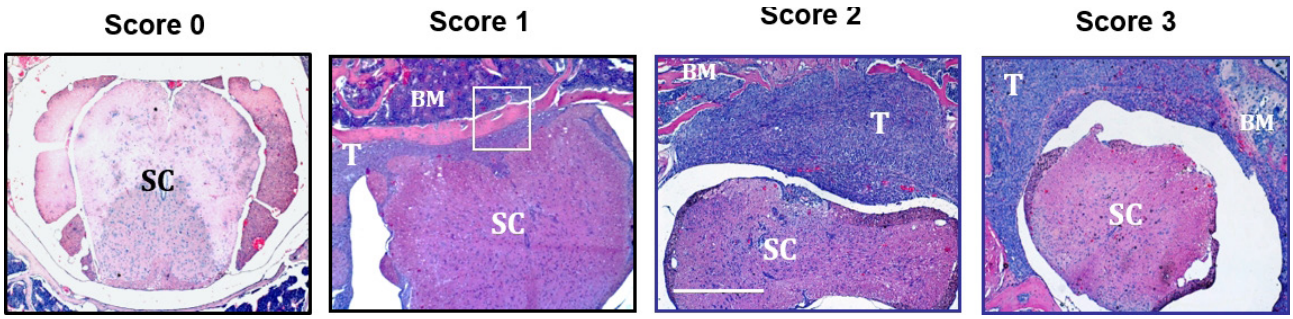

Figure 1 Histological analysis of axial cross sections of the spine. Mice inoculation of MDA-MB-231 cancer cells caused evolving neurological decline that was graded for: normal gait (Score 0, n = 2); asymmetrical gait (Score 1, n = 3), unilateral hind limb paralysis (Score 2, n = 3) and complete bilateral hind limb paralysis (Score 3, n = 3). Haematoxylin (nuclei=purple) and Eosin (cytoplasm=pink) staining of axial cross-sections of the mouse spine at each score. All Images are x5 magnification, scale bar represents 200 µm. Score 1 inset: tumour-bone interface. SC: spinal cord, BM: bone marrow, T: tumour.

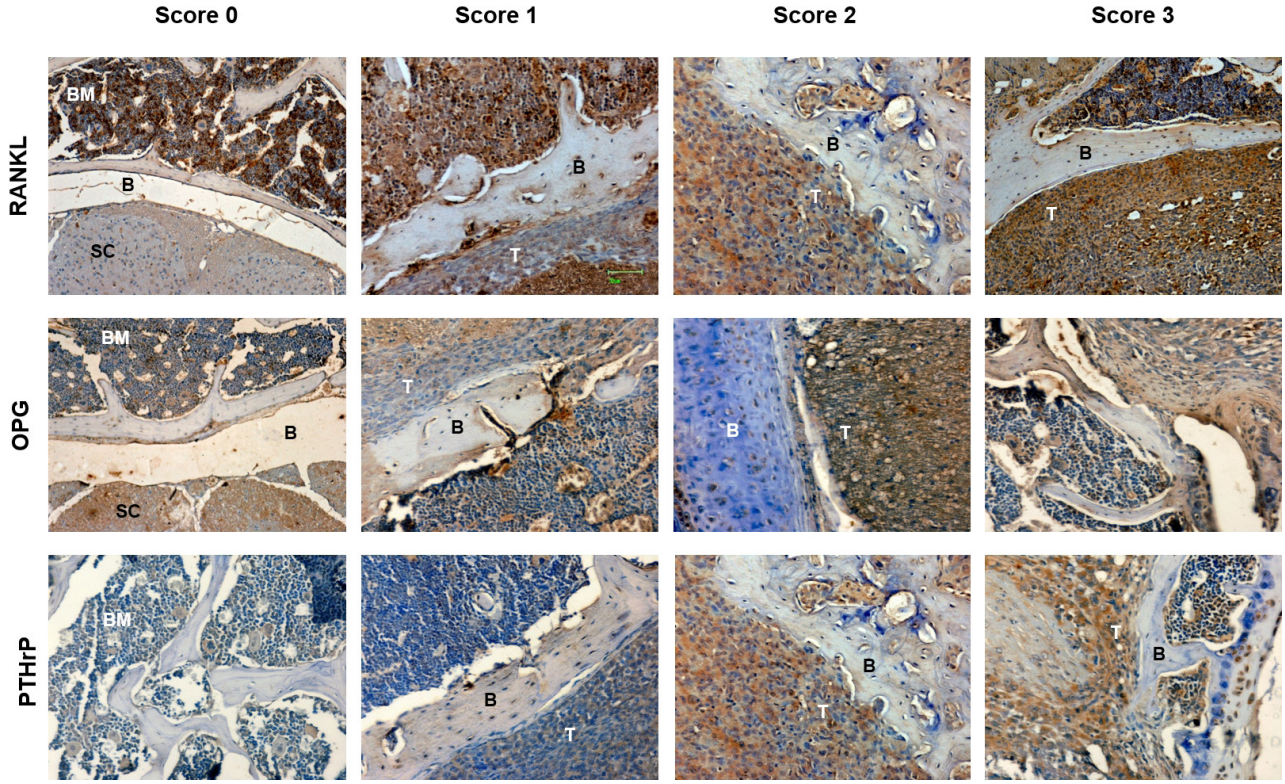

Figure 2 Immunohistochemical analysis. Expression of RANKL, OPG and PTHrP in MDA-MB-231-inoculated mouse spinal sections at corresponding scores 0-3. Brown staining represents positive expression. All Images are x20 magnification Scale bar represents 50 µm. BM: bone marrow, T: Tumour.

of RANKL and OPG expression with increasing tumour invasion (Figure 2). It must be noted that high baseline levels of RANKL compared to OPG and PTHrP were also observed in score 0 spinal sections. Statistical analysis showed a significant difference in score 3 RANKL and PTHrP expression when compared to score 0 ($p < 0.05$). Changes in OPG expression were observed in score 1 ($p < 0.01$), 2 ($p < 0.01$) and 3 ($p = 0.01$) spinal sections. An increase in RANKL expression was observed mainly in the invading tumour region, bone marrow and most prominently at the tumour-bone interface (arrows). Similarly, increased OPG and PTHrP expression was observed in the invading tumour region within the spinal canal and surrounding regions. Minimal background staining was observed in IgG stained negative controls (data not shown).

Immunohistochemical analysis of MMP-9, VEGF and IL-6 expression in MDA-MB-231-inoculated mouse spinal sections

A significant correlation between disease progression and increasing VEGF and IL-6 expression was observed from immunohistochemical analysis (Figure 3). An increase in VEGF expression was observed from score 1 ($p < 0.05$), 2 ($p < 0.05$) and 3 ($p = 0.05$). Positive staining was localised to regions of extensive tumour growth near the SC, however not within the bone marrow. IL-6 expression was minimal in the bone marrow in score 0 and increased upon neurological decline and scoring (score 3; $p < 0.05$). In addition, IL-6 expression was present at the tumour-bone interface and within tumour regions adjacent to the bone and bone marrow at scores 1-3. MMP-9 demonstrated a gradual increase in expression with higher tumour grades also, with major differences at the tumour-bone interface and within the growing tumour surrounding bone marrow and SC. This was significant in score 3 ($p < 0.01$). Minimal background was observed in all IgG stained negative controls (data not shown).

Flow cytometric and gene expression analysis of intracellular proteins in MDA-MB-231, MDA-MB-453 and MCF-7 cell lines

RT-PCR analysis of MDA-MB-231, MDA-MB-453 and MCF-7 cell lysates revealed visible mRNA bands and confirmed the genomic expression of all six tumour and bone-derived markers: RANKL (412 bp), OPG (324 bp), MMP-9 (172 bp), PTHrP (285 bp), VEGF

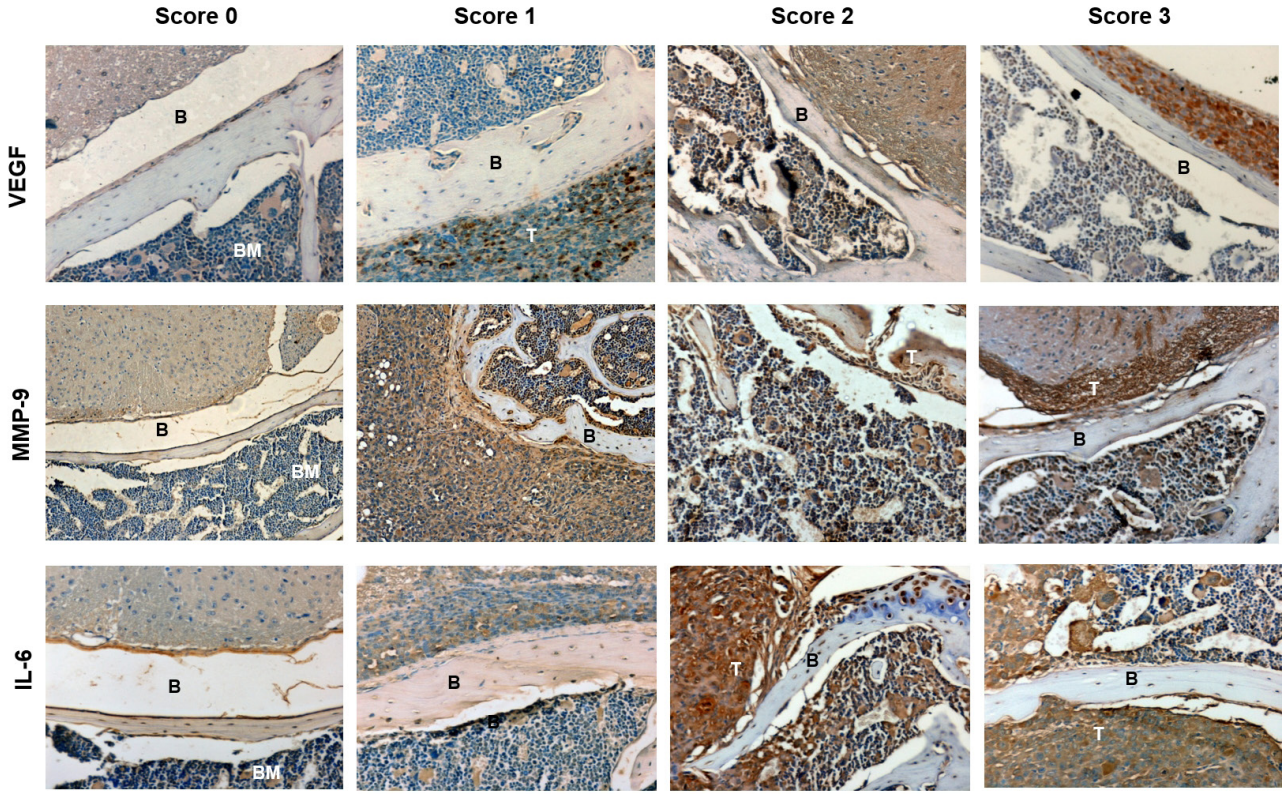

Figure 3 Immunohistochemical analysis. Expression of VEGF, MMP-9 and IL-6 in MDA-MB-231-inoculated mouse spinal sections at corresponding scores 0-3. Brown staining represents positive expression. All Images are x20 magnification Scale bar represents 50 µm. BM: bone marrow, T: Tumour, B: Bone.

(isoforms 404, 536 and 608 bp) and IL-6 (479 bp) (Figure 4). Analysis of intracellular protein expression by flow cytometry revealed high expression of RANKL, MMP-9, VEGF and IL-6 markers in MDA-MB-231, MDA-MB-453 and MCF-7 cells (Figure 5). Results are presented as histograms displaying positive population shifts in coloured fluorescence peaks relative to black peaks that represent IgG treated samples. Of note, both OPG and PTHrP demonstrated reduced or almost no expression ($p > 0.05$), as shown by the overlapping fluorescence peaks with their respective negatives for each of the lines. Both VEGF and IL-6 are shown to have the highest intracellular expression levels ($p < 0.05$) relative to other markers assessed.

Effects of ZA and Sorafenib on proliferation of MDA-MB-231, MDA-MB-453 and MCF-7 cell lines

Anti-proliferative and anti-metabolic effects of ZA and Sorafenib on MDA-MB-231, MDA-MB-453 and MCF-7 cells were analysed using CFSE and WST-1 assays in vitro (Figure 6). Both techniques displayed normal proliferation of untreated viable cells for five consecutive days, displayed by shifting fluorescence of CFSE labelled cells from all lines and a consistent increase in WST-1 absorbance for MDA-MB-453 and MCF-7 cells. Day 3 for ZA and day 1 for Sorafenib were chosen to be optimum for analysing treatment effects at various concentrations. After ZA treatment, maximum loss of division occurred on day 3 (72 hours) at 100 µM concentration, which is shown by the reduction in mean fluorescence (FITC). Reduction in proliferation was 52% for MDA-MB-231 (Ai), 63% for MDA-MB-453 (Aii) and 35% for MCF-7 (Aiii). However, the WST-1 assay failed to exhibit a dose-dependent effect of increasing ZA concentrations on the viability of these cells. Based on the WST-1 proliferation assay for Sorafenib, significant dose-dependent reduction in viability and metabolic activity was observed in MDA-MB-231 (Bi) and MDA-MB-453 (Bii) cells at 20 µM and 50 µM concentrations on

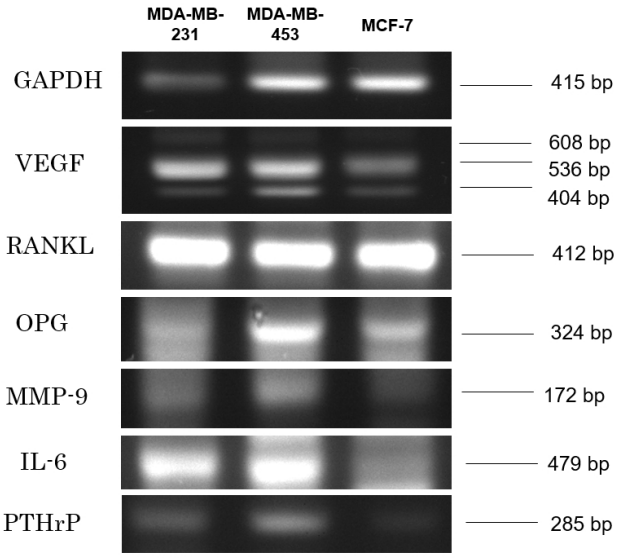

Figure 4 RT-PCR. Expression analysis of cell lysates for RANKL, OPG, MMP-9, PTHrP, VEGF and IL-6 markers. GAPDH was used as a positive control.

day 3. In comparison, it exhibited minimal effect on MCF-7 (Biii) cells over 96 hours. Further treatment analyses were carried out at 50 µM and 100 µM concentrations for ZA and at 20 µM and 50 µM concentrations for Sorafenib.

Effects of ZA and Sorafenib on apoptosis of MDA-MB-231, MDA-MB-453 and MCF-7 cell lines

ZA and Sorafenib treated cells were further assessed for anti-apoptotic effects by flow cytometry (Figure 7). Annexin V-FITC positive cells (Q1) were assessed as apoptotic, PI stained cells (Q4) necrotic, double stained cells (Q2) were late apoptotic or necrotic

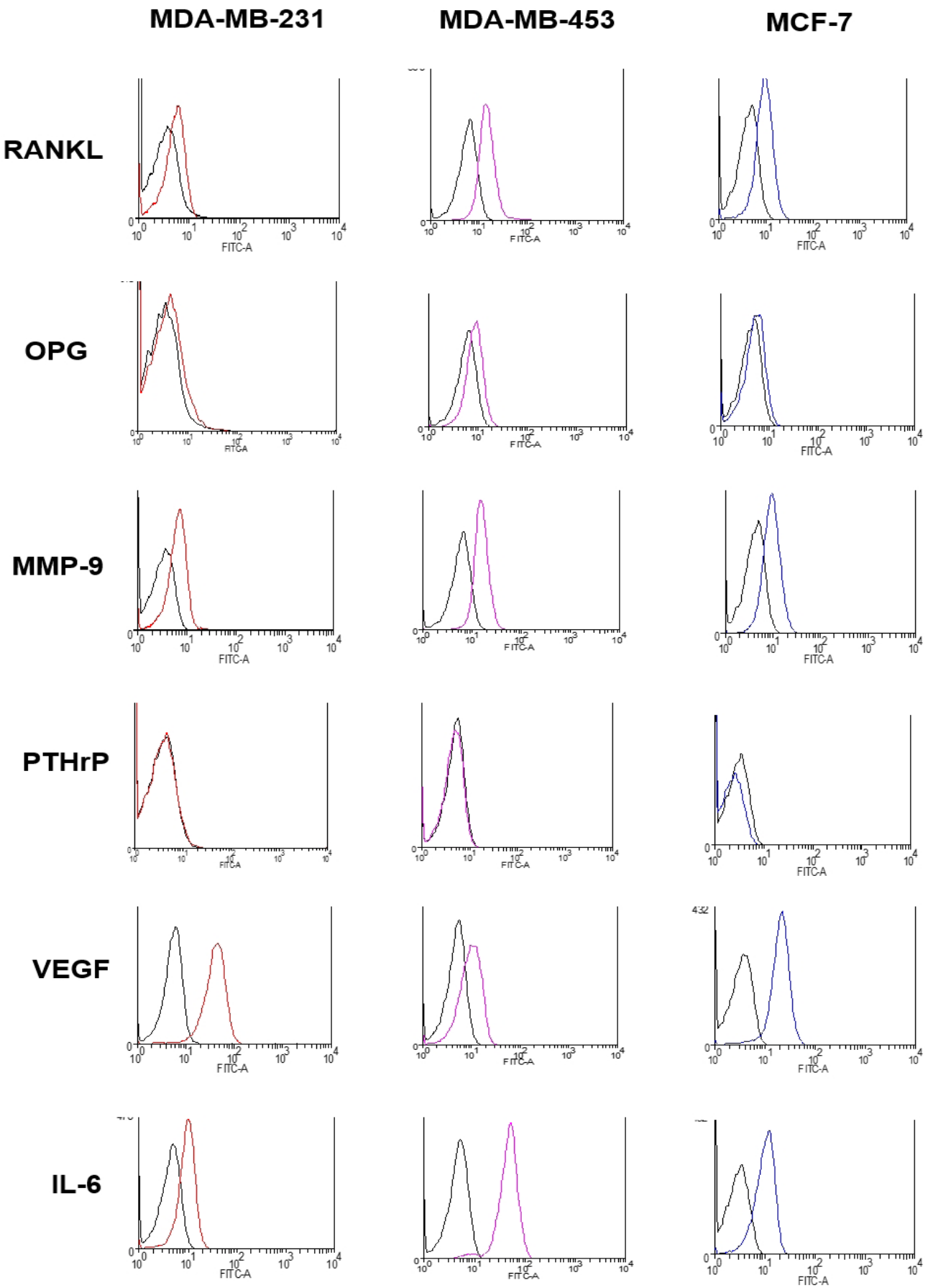

Figure 5 Intracellular protein expression. Protein expression of RANKL, OPG, MMP-9, PTHrP, VEGF and IL-6 in MDA-MB-231, MDA-MB-453 and MCF-7 cells via flow cytometry. Black peaks represent the IgG-treated samples (negative control), red, pink and blue peaks represent measured fluorescence of the markers. Representative flow cytometry data are shown from multiple experiments.

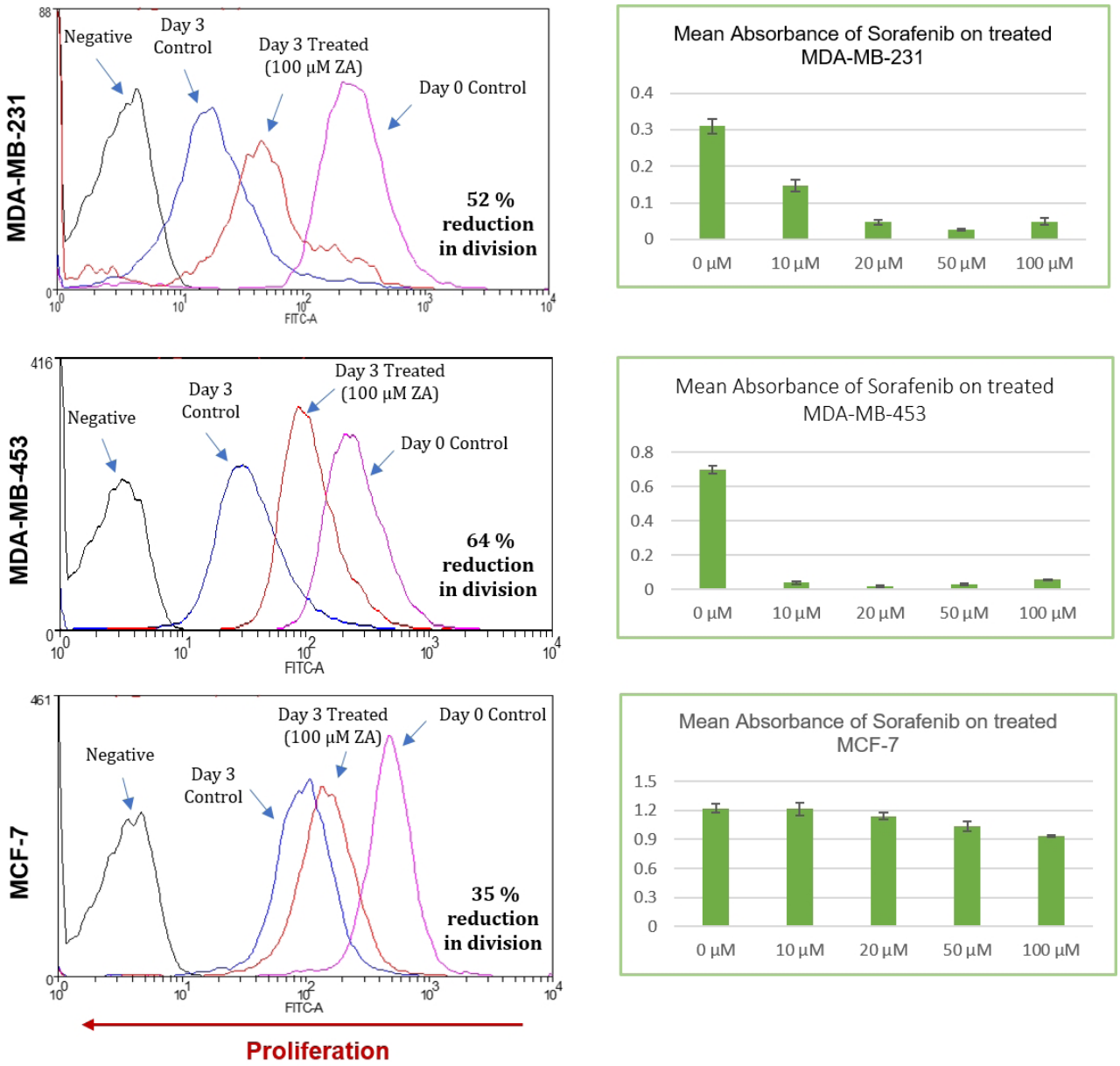

Figure 6 CFSE. Proliferation (left column) in ZA-treated MDA-MB-231, MDA-MB-453 and MCF-7 cells by flow cytometry. Cells were analysed after 72 hours of treatment. Fluorescence peaks in black represent unlabelled and untreated samples. Pink peaks represent labelled and untreated samples on day 0. Blue peaks represent labelled untreated samples on day 3. Red peaks represent labelled ZA-treated samples on day 3. WST-1 analysis (right column) for viability of Sorafenib treated MDA-MB-231, MDA-MB-453 and MCF-7 cells. Absorbance readings taken after treatment for four consecutive days at 0 – 100 µM concentrations. Representative results from multiple experiments are shown for both assays.

and cells negative for both stains (Q3) were viable. The bar graphs present mean percentage apoptosis at different drug concentrations. From analysis, Sorafenib exhibited an effective dose-dependent effect on apoptosis that was significant ($p < 0.05$) in both MDA-MB-231 (57.6%) and MDA-MB-453 (43%) cells at 20 µM and 50 µM concentrations (Figure 7). This was evident from the shift of MDA-MB-231 and MDA-MB-453 cell proportions from Q3 (negative for both apoptosis and necrosis) to Q1 (apoptosis) and Q2 (necrosis). A non-significant ($p > 0.05$) effect on apoptosis was observed in MCF-7 cells (data not shown). Additionally, ZA had no significant effect on apoptosis at 50 µM or 100 µM concentrations in MDA-MB-231, MDA-MB-453 or MCF-7 cells.

Effects of ZA and Sorafenib on the cytoplasmic expression of RANKL, MMP-9, VEGF and IL-6 in vitro

The effect of ZA and Sorafenib on the cytoplasmic expression of RANKL, MMP-9, VEGF and IL-6 was assessed in MDA-MB-231, MDA-MB-453 and MCF-7 cells by flow cytometry. Based on fluorescence readings and statistical analysis of treated and untreated cell samples, ZA and Sorafenib treatment did not induce any significant change in the level of intracellular expression of RANKL, MMP-9, VEGF or IL-6 proteins on day 3 for all cell lines. Representative histogram results are shown for ZA-treated (100 µM) and Sorafenib-treated (50 µM) MDA-MB-231 cells only (Figure 8).

DISCUSSION

The in vivo mouse model of intraosseous spinal cancer allows pre-clinical analysis of temporo-spatial pattern of breast cancer growth and invasion within the spine. Histological analysis of spinal cross-sections from normal mice and mice developing gradual paralysis demonstrated gradual invasion of MDA-MB-231 tumours towards

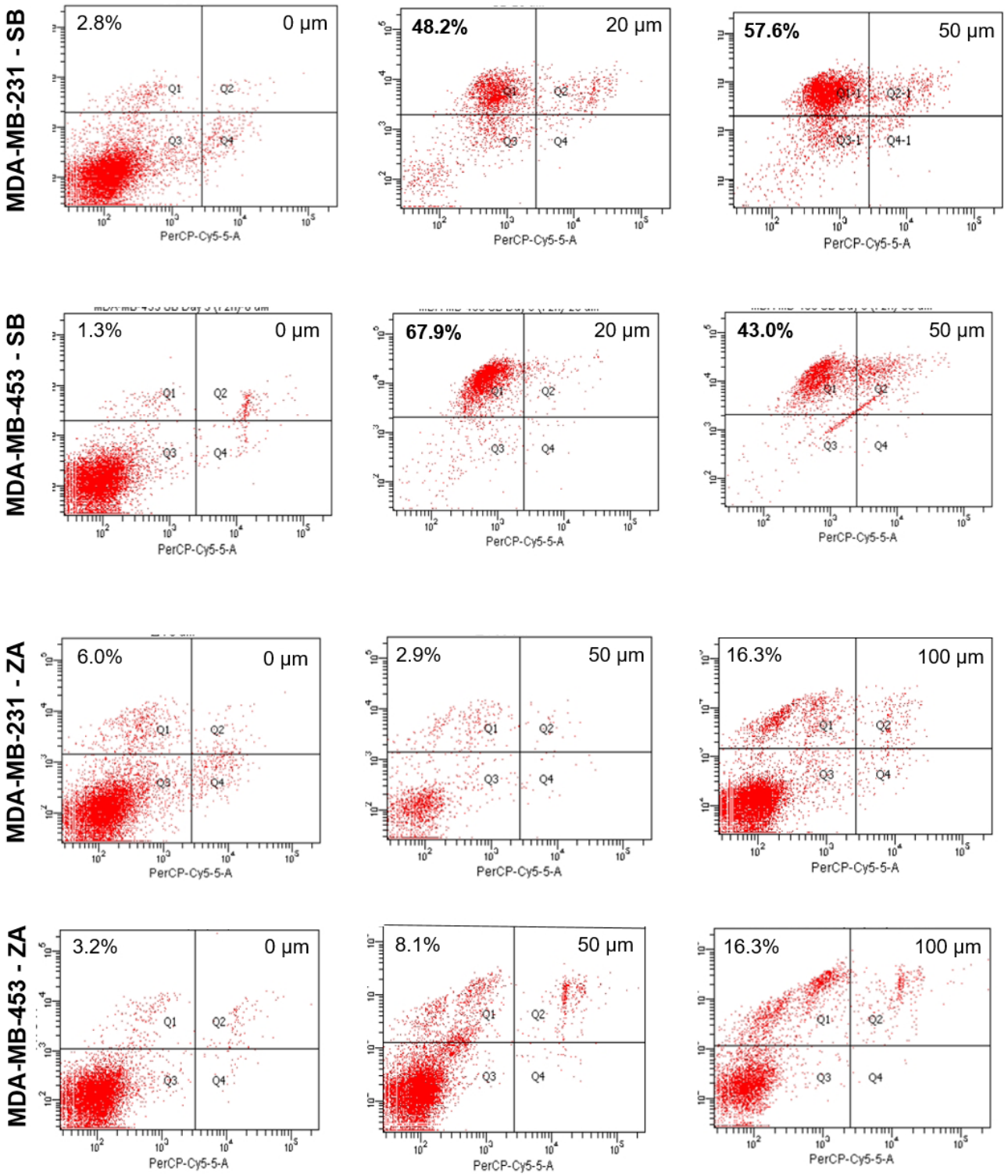

Figure 7 Annexin V staining. Quantitation of apoptosis in MDA-MB-231, MDA-MB-453 and MCF-7 cells via flow cytometry following Sorafenib (0, 20 and 50 µM) and ZA (0, 50 and 100 µM) treatment for 72 hours. Representative dot plots from multiple experiments are shown. Apoptosis is indicated by shifts from Q3 to Q1 (Annexin V-positive). Bar graphs present the mean percentage apoptosis (± SEM). SB: Sorafenib; ZA: Zoledronic Acid.

the spinal cord, causing its compression and destruction of the surrounding tissue structures. For investigating the underlying mechanisms of bone metastasis, we characterised the expression of six key bone and tumour markers within these spinal tissues containing MDA-MB-231 tumour. For in vitro analysis, we chose secondary triple negative breast cancer, MDA-MB-231, MDA-MB-453, and estrogen receptor-positive MCF-7 cells.

Among the six examined markers, we demonstrated that VEGF has the highest cytoplasmic expression in all three cell lines. Positive genetic expression as mRNA was observed for all proteins based on RT-PCR. Immunohistochemical analysis of scored spinal sections demonstrated significantly high VEGF expression in the invading tumour with intense localisation at the region of the tumour-bone interface lining the vertebral body. There would be an

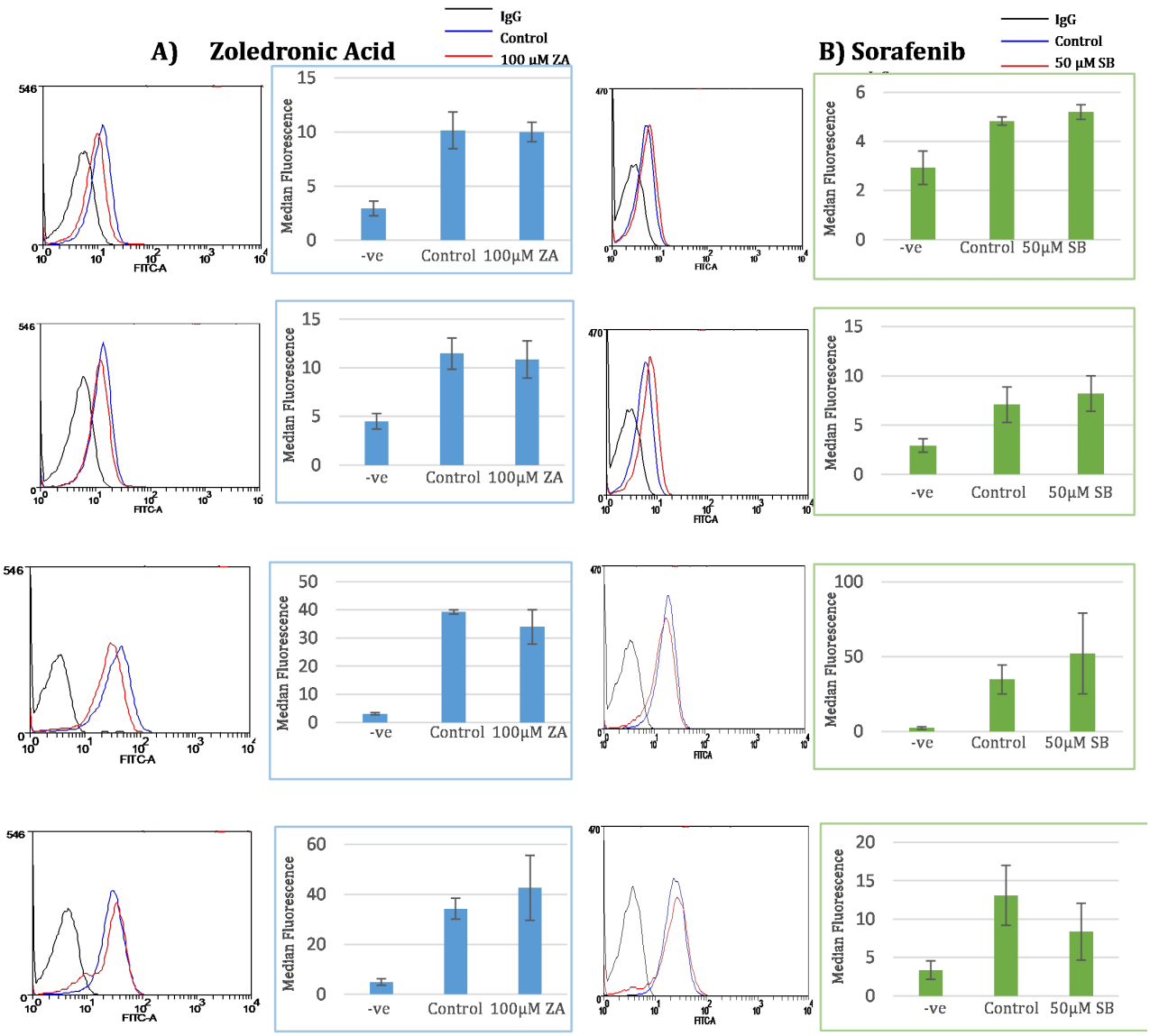

Figure 8 Intracellular flow cytometry analysis of RANKL, MMP-9, VEGF and IL-6 proteins in MDA-MB-231 cells after A) 100 µM ZA and B) 50 µM Sorafenib treatments after 72 hours. The peaks in black represent the background binding from IgG (negative), the peaks in blue represent normal expression of the examined markers, while the red peaks represent their expression following treatment. Quantification of median fluorescence are shown in the right-hand panels. For MDA-MB-231, non-significant ($p > 0.05$) expression for RANKL, MMP-9, IL-6 and VEGF were observed. Similar results were observed in other cell lines. Representative results are shown from multiple experiments. SB=Sorafenib; ZA=Zoledronic Acid

obvious role of physiological bone environment in inducing such excessive VEGF expression as it has been shown to be crucial for developing pro-angiogenic and distinct colonisation characteristics by creating favourable environment for tumour growth, angiogenesis and the vicious cycle of interactions in vivo[18,19]. Data from MMP-9 analysis also reveals significant intracellular expression in examined tumour cells and in score 3 spinal tissues. Importantly, our analysis revealed a high correlation of both VEGF and MMP-9 expression with increased tumour invasion and disease progression at the tumour-bone interface. Such evidence of an association in vivo is consistent with other findings that reported a relationship between VEGF over-expression and development of aggressive tumours, increased probability of metastasis, poor treatment response and reduced survival[20]. In other MDA-MB-231-induced tumours, MMP-9 expression is predominantly increased where it functions as a pro-angiogenic protease and promotes angiogenesis by causing VEGF mobilisation[21]. This is supported by our observation of concomitant localisation of MMP-9, RANKL and VEGF throughout our investigation. Based on these findings, MMP-9 and VEGF are vital for driving the invasive and aggressive metastatic propensities and therefore, MMP-9 is a potential therapeutic target for adjunctive anti-metastatic therapies.

We further characterised the expression of RANKL and OPG on the scored spinal tissues as they principally regulate osteoclast activity and subsequent bone degradation during osteolytic cancer progression. One of the most striking findings of our study is the graded increase of RANKL and OPG expression with increasing tumour scores from immunohistochemistry. High basal levels of RANKL (score 0) were observed in the bone marrow and significant localisation of RANKL and OPG was observed within the metastasised tumours across the bone in higher tumour grades. A supported finding by Blake et al. (2014) presented evidence of RANKL expressing cells at the tumour-bone interface adjacent to osteoclasts, which has been clearly associated with tumour-promoted osteolysis[4,13]. This essentially correlates with our findings from the TRAP assay that displayed significant increase in osteoclast recruitment within the invad-

ing tumour between bone and the spinal cord. Thus, the progressive neurological dysfunction observed in our model can be associated with increasing osteolysis. Evidently, chemotactic role of RANKL further causes migration of RANKL-expressing tumour and epithelial cells to the bone microenvironment, causing enhanced RANKL/RANK interactions and osteoclast accumulation on bone surface[22]. This suggests that more prominent osteolysis and tumour invasion occurs at the tumour-bone interface than within the bone marrow. Such extensive protein expression during disease progression in vivo may be from RANKL positive MDA-MB-231 tumour and existing stromal cells, or from the influence of other bone microenvironment factors during secondary osteoclastogenesis[4]. Simultaneous increase in OPG expression in mice scored 2 and 3 possibly indicates its physiological upregulation for reversal in the effects of excess RANKL/RANK interaction and osteoclastogenesis. Surprisingly, studies have also identified OPG as a contributing factor for the predisposition of osteolysis and bone metastasis, where it increases RANKL production and enhances survival of MDA-MB-231 tumours[23]. Collectively, our characterisation of RANKL and OPG in MDA-MB-231 tumours re-emphasises the significance of tumour-stromal interactions and osteoclast-mediated bone destruction during phenotypical osteolytic metastasis. RANKL expression, which was dominant on the spinal sections and in vitro, deserves attention as it has consistently been correlated with increased production of osteolytic factors, reduced bone density in different model systems and advancement of other metastasis pathways[4].

PTHrP, another key osteolytic factor had increased expression with the development of paralysis despite no cytoplasmic expression in cultured tumour cells, based on immunohistochemical characterisation. A possible reason behind this can be the induced expression of PTHrP by the complex bone and tumour interactions since a number of immunohistochemical and clinical BC studies demonstrated prominent PTHrP localisation at the site of bone metastasis[24,25]. An important interacting factor can be the inflammatory marker IL-6, which demonstrated consistently high expression in the examined tumour cells as well as on the spinal sections. According to a number of in vitro and in vivo studies, IL-6 over-expression promotes a hypoxic and treatment-resistant invasive phenotype of tumour cells[26,27]. Our observation of significant PTHrP expression in score 3 corresponds with that of RANKL expression and this may suggest their collective activity in augmenting osteolytic signalling pathways for bone degradation. Also, both these proteins showed similar localisation to RANKL and other markers at the tumour-bone interface, which suggests that IL-6 contributes to the tumour-promoting functions of other factors. It has been documented that IL-6 and PTHrP enhances the bone and stromal upregulation of RANKL, and together mediate further interactions to promote excessive bone resorption, osteoclastogenesis and metastatic BC growth within the bone[28,29]. The expression of VEGF in our study can be explained by the ability of IL-6 to promote stimulation of angiogenesis and inhibit apoptosis[13]. This data supports the idea that IL-6 can directly affect the growth of breast cancer and cause spontaneous bone metastasis[13,14]. Overall, extensive tumour and stromal expression of IL-6 along with RANKL and VEGF in vivo and in vitro suggest that tumour-induced changes in the bone microenvironment are considerably linked to mechanisms of bone turnover as well as tumour progression.

The presence of MDA-MB-231 tumour and bone-derived markers, VEGF, RANKL and IL-6 during progressive spinal cord compression provides evidence of complex tumour and stromal interactions within the spine, thus facilitating metastasis development and favouring cancer growth, invasion, bone break-down and apoptosis in the tumour-bone microenvironment. Therefore, therapies targeting mechanisms of angiogenesis and bone degradation specifically are necessary for inhibiting aggressive tumour spread and bone damage, thus we chose ZA and Sorafenib for this purpose. Investigating potential inhibitory effects of these drugs on the same tumour cells in vitro is preliminary for elucidating their physiological effect on tumour growth and invasion in vivo. This is crucial for further understanding spinal metastasis mechanisms.

In our preliminary treatment studies, Sorafenib and ZA have been assessed for their potential anti-proliferative and apoptotic effects on cultured MDA-MB-231, MDA-MB-453 and MCF-7 cancer cells. We observed that ZA causes a significant reduction in normal proliferation of these cells and this is consistent with the study by Beleut et al. (2010)[14]. Significant reduction in growth and viability, and increased apoptosis of MDA-MB-231 and MDA-MB-453 tumour cells was also demonstrated by experiments using Sorafenib. Its cytotoxic effect on mitochondrial activity, based on WST-1 assay, is consistent with other analyses of MDA-MB-231 and MCF-7 cells, where diminished mitochondrial function caused pronounced generation of reactive oxygen species (ROS) that led to cell death[30,31]. Numerous studies have revealed that these anti-proliferative, apoptotic and cytotoxic effects of these drugs are linked to the significant suppression of RTKs and other signalling pathways including Ras/Raf/MAPK/Akt and PI3K/Akt/mTORC1 cascades, and downstream cell-cycle and anti-apoptotic regulatory factors[32,33,34]. Without treatment, these are usually abnormally activated for promoting malignancy and preventing apoptosis. Possible interactions among RTKs and hormone receptors may explain the resistance observed in MCF-7 cells towards Sorafenib.

Anti-cancer effects of ZA in vitro and in animal model systems have shown to include anti-proliferative, anti-angiogenic, anti-invasive and immunomodulatory effects and many of these are clinically relevant[35]. Thus, Sorafenib and ZA have been assessed for their effect on tumour-bone derived markers for further investigating their efficacy in inhibiting metastasis-related osteolytic and angiogenic mechanisms, which may delay disease progression. However, we observed that neither drugs change the expression of RANKL, MMP-9, VEGF and IL-6 proteins that are highly present in the cytoplasm, although they demonstrated an anti-proliferative effect on these cancer cells. Such observations may suggest that the signalling pathways inhibited by ZA (melvonate pathway) and Sorafenib (RTK) do not directly interfere with cytoplasmic transcription and expression of RANKL, MMP-9, VEGF and IL-6. This can also be explained by the mechanism of resistance, whereby tumour cells circumvent the drugs' reducing effects by consistently secreting these osteolytic factors, which helps them maintain a tumour-promoting phenotype. Therefore, since ZA exerts multi-directional effects through the melvonate pathway at different stages of tumour growth, more extensive modulatory treatment is required to interfere with intracellular protein expression and apoptotic mechanisms. Essentially, ZA and Sorafenib have both been effective in suppressing angiogenic responses, osteoclast activity and BC tumour growth by modifying VEGF, MMP-9 and RANKL and IL-6 expression, as reported by numerous in vivo and clinical studies[36,37,38,39,40]. This suggests that both ZA and Sorafenib are capable of altering the expression of metastasis-promoting proteins. Further investigations of these drugs in a physiological setting are required, where potential targeted inhibitory effects can modulate the tumour environment. Future clinical and translational research on their anti-cancer efficacy at metastatic locations can be more effective in providing answers to yet unclear mechanisms of action.

ACKNOWEDGMENTS

This work was supported by funding from the Victorian Orthopaedic Research Trust, Medtronic Australasia Pty Ltd and Johnson & Johnson Medical Pty Ltd. Cell lines were generously provided by John Mariadason from Ludwig Institute of Medical Research, Heidelberg, Australia and Stephen Fox from the Peter MacCallum Cancer Centre, Parkville, Australia.

REFERENCES

1. Polascik TJ, Mouraviev V. Zoledronic acid in the management of metastatic bone disease. Ther Clin Risk Manag. 2008 Feb;4(1):261-8. [PMID: 18728715]; [DOI: 10.2147/tcrm.s2707].
2. Cossigny D, Quan GM. In vivo animal models of spinal metastasis. Cancer Metastasis Rev. 2012 Jun;31(1-2):99-108. [PMID: 22090011]; [DOI: 10.1007/s10555-011-9332-x].
3. Cossigny DA, Mouhtouris E, Dushyanthen S, Gonzalvo A, Quan GM. An in vivo mouse model of intraosseous spinal cancer causing evolving paraplegia. J Neurooncol. 2013 Nov;115(2):189-96. [PMID: 23955595]; [DOI: 10.1007/s11060-013-1226-z].
4. Blake ML, Tometsko M, Miller R, Jones JJ, Dougall WC. RANK expression on breast cancer cells promotes skeletal metastasis. Clin Exp Metastasis. 2014 Feb;31(2):233-45. [PMID: 24272640]; [DOI: 10.1007/s10585-013-9624-3].
5. Dougall WC. RANKL signaling in bone physiology and cancer. Curr Opin Support Palliat Care. 2007 Dec;1(4):317-22. [PMID: 18685382]; [DOI: 10.1097/SPC.0b013e3282f335be].
6. Yoneda T, Tanaka S, Hata K. Role of RANKL/RANK in primary and secondary breast cancer. World J Orthop. 2013 Oct 18;4(4):178-85. [PMID: 24147253]; [DOI: 10.5312/wjo.v4.i4.178].
7. O'Keefe RJ, Guise TA. Molecular mechanisms of bone metastasis and therapeutic implications. Clin Orthop Relat Res. 2003 Oct(415 Suppl):S100-4. [PMID: 14600598]; [DOI: 10.1097/01.blo.0000093847.72468.2f].
8. Guise TA, Mohammad KS, Clines G, Stebbins EG, Wong DH, Higgins LS, Vesella R, Corey E, Padalecki S, Suva L, Chirgwin JM. Basic mechanisms responsible for osteolytic and osteoblastic bone metastases. Clin Cancer Res. 2006 Oct 15;12(20 Pt 2):6213s-6216s. [PMID: 17062703]; [DOI: 10.1158/1078-0432.CCR-06-1007].
9. Chaturvedi P, Gilkes DM, Wong CC, Luo W, Zhang H, Wei H, Takano N, Schito L, Levchenko A, Semenza GL. Hypoxia-inducible factor-dependent breast cancer-mesenchymal stem cell bidirectional signaling promotes metastasis. J Clin Invest. 2013 Jan;123(1):189-205. [PMID: 23318994]; [DOI: 10.1172/JCI64993].
10. Schneider BP, Miller KD. Angiogenesis of breast cancer. J Clin Oncol. 2005 Mar 10;23(8):1782-90. [PMID: 15755986]; [DOI: 10.1200/JCO.2005.12.017].
11. Abedin M, King N. Diverse evolutionary paths to cell adhesion. Trends Cell Biol. 2010 Dec;20(12):734-42. [PMID: 20817460]; [DOI: 10.1016/j.tcb.2010.08.002].
12. Guise TA, Chirgwin JM. Transforming growth factor-beta in osteolytic breast cancer bone metastases. Clin Orthop Relat Res. 2003 Oct(415 Suppl):S32-8. [PMID: 14600590]; [DOI: 10.1097/01.blo.0000093055.96273.69].
13. Guo Y, Xu F, Lu T, Duan Z, Zhang Z. Interleukin-6 signaling pathway in targeted therapy for cancer. Cancer Treat Rev. 2012 Nov;38(7):904-10. [PMID: 22651903]; [DOI: 10.1016/j.ctrv.2012.04.007].
14. Beleut M, Rajaram RD, Caikovski M, Ayyanan A, Germano D, Choi Y, Schneider P, Brisken C. Two distinct mechanisms underlie progesterone-induced proliferation in the mammary gland. Proc Natl Acad Sci U S A. 2010 Feb 16;107(7):2989-94. [PMID: 20133621]; [DOI: 10.1073/pnas.0915148107].
15. Hibberd C, Cossigny DA, Quan GM. Animal cancer models of skeletal metastasis. Cancer Growth Metastasis. 2013;6:23-34. [PMID: 24665205]; [DOI: 10.4137/CGM.S11284].
16. Gnant M, Balic M, Petru E, Raunki W, Singer CF, Steger GG, Watzke IM, Brodowicz T. Treatment of Bone Metastases in Patients with Advanced Breast Cancer. Breast Care (Basel). 2012 Apr;7(2):92-98. [PMID: 22740794]; [DOI: 10.1159/000338650].
17. Kristensen TB, Knutsson ML, Wehland M, Laursen BE, Grimm D, Warnke E, Magnusson NE. Anti-vascular endothelial growth factor therapy in breast cancer. Int J Mol Sci. 2014 Dec 11;15(12):23024-41. [PMID: 25514409]; [DOI: 10.3390/ijms151223024].
18. Bender RJ, Mac Gabhann F. Expression of VEGF and semaphorin genes define subgroups of triple negative breast cancer. PLoS One. 2013;8(5):e61788. [PMID: 23667446]; [DOI: 10.1371/journal.pone.0061788].
19. Ruan Q, Han S, Jiang WG, Boulton ME, Chen ZJ, Law BK, Cai J. alphaB-crystallin, an effector of unfolded protein response, confers anti-VEGF resistance to breast cancer via maintenance of intracrine VEGF in endothelial cells. Mol Cancer Res. 2011 Dec;9(12):1632-43. [PMID: 21984182]; [DOI: 10.1158/1541-7786.MCR-11-0327].
20. Bahhnassy A, Mohanad M, Shaarawy S, Ismail MF, El-Bastawisy A, Ashmawy AM, Zekri A. Transforming growth factor-beta, insulin-like growth factor I/insulin-like growth factor I receptor and vascular endothelial growth factor-A: prognostic and predictive markers in triple-negative and non-triple-negative breast cancer. Mol Med Rep. 2015 Jul;12(1):851-64. [PMID: 25824321]; [DOI: 10.3892/mmr.2015.3560].
21. Ahn GO, Brown JM. Matrix metalloproteinase-9 is required for tumor vasculogenesis but not for angiogenesis: role of bone marrow-derived myelomonocytic cells. Cancer Cell. 2008 Mar;13(3):193-205. [PMID: 18328424]; [DOI: 10.1016/j.ccr.2007.11.032].
22. Jones DH, Nakashima T, Sanchez OH, Kozieradzki I, Komarova SV, Sarosi I, Morony S, Rubin E, Sarao R, Hojilla CV, Komnenovic V, Kong Y, Schreiber M, Dixon SJ, Sims SM, Khokha R, Wada T, Penninger JM. Regulation of cancer cell migration and bone metastasis by RANKL. Nature. 2006 Mar 30;440(7084):692-6. [PMID: 16572175]; [DOI: 10.1038/nature04524].
23. Neville-Webbe HL, Cross NA, Eaton CL, Nyambo R, Evans CA, Coleman RE, Holen I. Osteoprotegerin (OPG) produced by bone marrow stromal cells protects breast cancer cells from TRAIL-induced apoptosis. Breast Cancer Res Treat. 2004 Aug;86(3):269-79. [PMID: 15567943]; [DOI: 10.1023/b:brea.0000036900.48763.b3]
24. Soki FN, Park SI, McCauley LK. The multifaceted actions of PTHrP in skeletal metastasis. Future Oncol. 2012 Jul;8(7):803-17. [PMID: 22830401]; [DOI: 10.2217/fon.12.76].
25. Boras-Granic K, Wysolmerski JJ. PTHrP and breast cancer: more than hypercalcemia and bone metastases. Breast Cancer Res. 2012 Apr 25;14(2):307. [PMID: 22546075]; [DOI: 10.1186/bcr3129].
26. Liu L, Chen X, Wang Y, Qu Z, Zhao J, Yan X, Zhang H, Zhou Y. Notch3 is important for TGF-beta-induced epithelial-mesenchymal transition in non-small cell lung cancer bone metastasis by regulating ZEB-1. Cancer Gene Ther. 2014 Sep;21(9):364-72. [PMID: 25080992]; [DOI: 10.1038/cgt.2014.39].
27. Sosnoski DM, Norgard RJ, Grove CD, Foster SJ, Mastro AM. Dormancy and growth of metastatic breast cancer cells in a bone-like microenvironment. Clin Exp Metastasis. 2015 Apr;32(4):335-44. [PMID: 25749879]; [DOI: 10.1007/s10585-015-9710-9].
28. 28. Dougall WC. Molecular pathways: osteoclast-dependent and osteoclast-independent roles of the RANKL/RANK/OPG pathway in tumorigenesis and metastasis. Clin Cancer Res. 2012 Jan 15;18(2):326-35. [PMID: 22031096]; [DOI: 10.1158/1078-0432.

CCR-10-2507].

29. Xu M, Zheng YL, Xie XY, Lian JY, Pan FS, Zheng SG, Lu MD. Sorafenib blocks the HIF-1alpha/VEGFA pathway, inhibits tumor invasion, and induces apoptosis in hepatoma cells. DNA Cell Biol. 2014 May;33(5):275-81. [PMID: 24611881]; [DOI: 10.1089/dna.2013.2184].
30. Fumarola C, Caffarra C, La Monica S, Galetti M, Alfieri RR, Cavazzoni A, Galvani E, Generali D, Petronini PG, Bonelli MA. Effects of sorafenib on energy metabolism in breast cancer cells: role of AMPK-mTORC1 signaling. Breast Cancer Res Treat. 2013 Aug;141(1):67-78. [PMID: 23963659]; [DOI: 10.1007/s10549-013-2668-x].
31. Carloni S, Fabbri F, Brigliadori G, Ulivi P, Silvestrini R, Amadori D, Zoli W. Tyrosine kinase inhibitors gefitinib, lapatinib and sorafenib induce rapid functional alterations in breast cancer cells. Curr Cancer Drug Targets. 2010 Jun;10(4):422-31. [PMID: 20384581]; [DOI: 10.2174/156800910791208580].
32. Dunn LK, Mohammad KS, Fournier PG, et al. Hypoxia and TGF-beta drive breast cancer bone metastases through parallel signaling pathways in tumor cells and the bone microenvironment. PLoS One. 2009 Sep 3;4(9):e6896. [PMID: 20384581]; [DOI: 10.2174/156800910791208580].
33. Locatelli SL, Giacomini A, Guidetti A, Cleris L, Mortarini R, Anichini A, Gianni AM, Carlo-Stella C. Perifosine and sorafenib combination induces mitochondrial cell death and antitumor effects in NOD/SCID mice with Hodgkin lymphoma cell line xenografts. Leukemia. 2013 Aug;27(8):1677-87. [PMID: 23360848]; [DOI: 10.1038/leu.2013.28].
34. Bonelli MA, Fumarola C, Alfieri RR, La Minica S, Cavazzoni A, Galetti M, Gatti R, Belletti S, Harris AL, Fox SB, Evans DB, Dowsett M, Martin LA, Bottini A, Generali D, Petronini PG. Synergistic activity of letrozole and sorafenib on breast cancer cells. Breast Cancer Res Treat. 2010 Nov;124(1):79-88. [PMID: 20054642]; [DOI: 10.1007/s10549-009-0714-5].
35. Coleman R, Cook R, Hirsh V, Major P, Lipton A. Zoledronic acid use in cancer patients: more than just supportive care? Cancer. 2011 Jan 01;117(1):11-23. [PMID: 21235033]; [DOI: 10.1002/cncr.25529].
36. Ibrahim T, Liverani C, Mercatali L, Sacanna E, Zanoni M, Fabbri F, Zoli W, Amadori D. Cisplatin in combination with zoledronic acid: a synergistic effect in triple-negative breast cancer cell lines. Int J Oncol. 2013 Apr;42(4):1263-70. [PMID: 23403907]; [DOI: 10.3892/ijo.2013.1809].
37. Choi HN, Jin HO, Kim JH, Hong SE, Kim HA, Kim EK, Lee JK, Park IC, Noh WC. Inhibition of S6K1 enhances glucose deprivation-induced cell death via downregulation of anti-apoptotic proteins in MCF-7 breast cancer cells. Biochem Biophys Res Commun. 2013 Mar 01;432(1):123-8. [PMID: 23376066]; [DOI: 10.1016/j.bbrc.2013.01.074].
38. Casimiro S, Mohammad KS, Pires R, Tato-Costa J, Alho I, Teixeria R, Carvalho A, Ribeiro S, Lipton A, Guise TA, Costa L. RANKL/RANK/MMP-1 molecular triad contributes to the metastatic phenotype of breast and prostate cancer cells in vitro. PLoS One. 2013;8(5):e63153. [PMID: 23696795]; [DOI: 10.1371/journal.pone.0063153].
39. Massarweh S, Moss J, Wang C, Romond E, Slone S, Weiss H, Karabakhtsian RG, Napier D, Black EP. Impact of adding the multikinase inhibitor sorafenib to endocrine therapy in metastatic estrogen receptor-positive breast cancer. Future Oncol. 2014 Dec;10(15):2435-48. [PMID: 24826798]; [DOI: 10.2217/fon.14.99].
40. Roland CL, Lynn KD, Toombs JE, Dineen SP, Udugamasooriya DG, Brekken RA. Cytokine levels correlate with immune cell infiltration after anti-VEGF therapy in preclinical mouse models of breast cancer. PLoS One. 2009 Nov 03;4(11):e7669. [PMID: 19888452]; [DOI: 10.1371/journal.pone.0007669].